PHOTONICS Research

Emission spectroscopy of $NaYF_4$:Eu nanorods optically trapped by Fresnel lens fibers

Aashutosh Kumar,[1] Asa Asadollahbaik,[2] Jeongmo Kim,[3] Khalid Lahlil,[3] Simon Thiele,[4] Alois M. Herkommer,[4] Síle Nic Chormaic,[1,5] Jongwook Kim,[3] Thierry Gacoin,[3] Harald Giessen,[2] and Jochen Fick[1,*]

[1]Université Grenoble Alpes, CNRS, Institut Néel, 38000 Grenoble, France
[2]4th Physics Institute and Research Center SCoPE, University of Stuttgart, 70569 Stuttgart, Germany
[3]Université Paris Saclay, CNRS, Laboratoire de Physique de la Matière Condensée, École Polytechnique, 91128 Palaiseau, France
[4]Institute of Applied Optics and Research Center SCoPE, University of Stuttgart, 70569 Stuttgart, Germany
[5]Okinawa Institute of Science and Technology Graduate University, Okinawa 904-0495, Japan
*Corresponding author: jochen.fick@neel.cnrs.fr

Received 21 June 2021; revised 17 November 2021; accepted 18 November 2021; posted 22 November 2021 (Doc. ID 434645); published 11 January 2022

$NaYF_4$:Eu nanorods with high aspect ratios are elaborated and optically trapped using dual fiber optical tweezers in a counterpropagating geometry. High trapping efficiency is observed using converging beams, emitted from diffractive Fresnel lenses directly 3D printed onto cleaved fiber facets. Stable nanorod trapping and alignment are reported for a fiber-to-fiber distance of 200 μm and light powers down to 10 mW. Trapping of nanorod clusters containing one to three nanorods and the coupling of nanorod motion in both axial and transverse directions are considered and discussed. The europium emission is studied by polarization-resolved spectroscopy with particular emphasis on the magnetic and electric dipole transitions. The respective σ and π orientations of the different emission lines are determined. The angles with respect to the nanorod axes of the corresponding magnetic and electric dipoles are calculated. Mono-exponential emission decay with decay time of 4–5 ms is reported. It is shown that the nanorod orientation can be determined by purely spectroscopic means.

https://doi.org/10.1364/PRJ.434645

1. INTRODUCTION

Optical tweezers have become standard tools in many interdisciplinary research domains due to the possibility of manipulating, sorting, separating, and trapping micro- and nanometer sized objects. Already in 1993, shortly after the development of the original approach in 1986 based on strong laser beam focusing using a high numerical aperture (NA) microscope objective [1], the first fiber-based optical tweezers were demonstrated [2]. Trapping was obtained by aligning the fibers of two pigtailed lasers using just a cover slip and a capillary. This first work already highlights the great simplicity and small footprint of optical fiber tweezers. It has already been demonstrated that trapping of small particles at low light power is possible using microstructured fibers [3–5]. Chemical etching [6–10] and mechanical grinding [11] are the most popular techniques to realize fiber tips used for trapping in single or dual fiber geometries. More complex methods such as focused ion beam etching [12–14] and self-guided photopolymerization [15] are also applied to realize beam shaping devices at the distal ends of optical fibers. Finally, 3D printing of diffracting elements presents a versatile technique for beam shaping [16] and imaging purposes [17]. Fresnel lenses obtained by this technique have recently been applied for very efficient optical trapping of 1 μm and 500 nm polystyrene beads [18].

A major motivation for the development of optical tweezers is the possibility to combine trapping experiments with other experimental tools such as optical spectroscopy [19–22]. As an example, one can cite the use of Raman tweezers for the identification of nanoplastics in seawater [23]. Moreover, photoluminescent nanoparticle trapping is of great interest due to potential applications in bio-imaging experiments [24]. For example, $NaYF_4$ nanorods are biocompatible materials used as efficient hosts in optoelectronic devices [25,26]. $NaYF_4$ has a relatively low phonon energy (300–400 cm^{-1}) [27], and the presence of yttrium allows straightforward substitution with other lanthanide ions [28]. The red-emitting Eu^{3+} ions show interesting anisotropic emission that is more prominent than Er/Yb or other lanthanide dopants [29,30]. Moreover, the europium emission features distinct electric dipole (ED) and magnetic dipole (MD) transitions [27,31,32].

Optical trapping and manipulation require recording the position of trapped particles by optical microscopy. Photoluminescence (PL) imaging allows for determination of the nanoparticle position, whereas in the case of nanorods with hexagonal crystal structure, the emission anisotropy is used to determine the nanorod orientation [30,33,34]. Nanorods with high aspect ratios tend to form clusters that cannot be resolved optically. Measuring the PL emission power [33] or the trap stiffness [35] allows us, however, to estimate the number of nanorods in a cluster.

In this paper, we report on optical trapping of $NaYF_4$:Eu^{3+} nanorods using our recently developed Fresnel lens fibers [18]. These fibers produce focused beams with NA = 0.5 and a focal length of 100 μm. Compared to former experiments using optical fiber tips [36,37], the nanorods are efficiently trapped at about 100 μm from the fibers, thus removing any mechanical or optical influence on the particle's optical emission properties. Two specific aspects will be presented in detail: the optical trapping behavior of nanorods in the anisotropic trapping potential of our dual fiber tweezers and the spectroscopic investigation of the anisotropic europium emission.

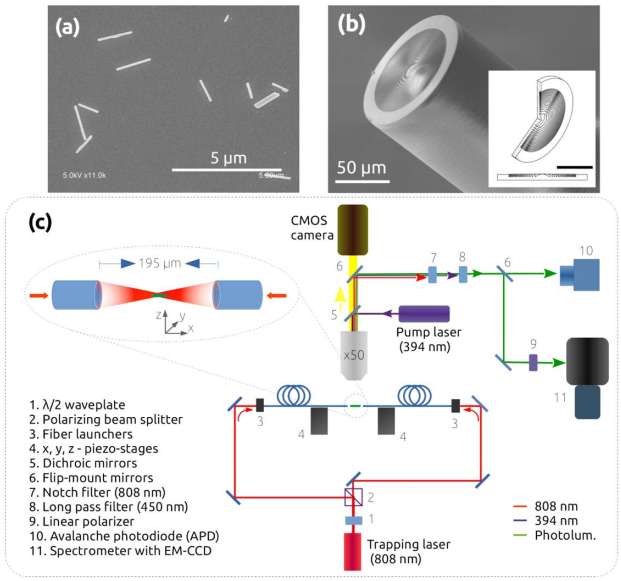

Fig. 1. (a) SEM image of $NaYF_4$:Eu^{3+} nanorods. (b) SEM image and CAD drawing of the Fresnel lens fiber. (c) Schematic of the optical fiber tweezers setup.

2. MATERIALS AND METHODS

A. Nanorod Synthesis

The $NaYF_4$:Eu^{3+} nanorods are synthesized by the hydrothermal process described in more detail in Ref. [37]. The process is based on a mixture of sodium hydroxide, ammonium fluoride, and rare earth chlorides in an oleic acid solution that is transferred into an autoclave and heated at 200°C for 24 h while stirring. The nanorods are obtained when cooling down to ambient temperature. After synthesis, particles are extensively washed by centrifugation to remove excess oleic acid, and surface oleate ligands are exchanged with citrates to ensure good dispersion. Just before optical trapping experiments, the nanorod solution is extensively diluted in water and sonicated for a few minutes to separate the nanorods. The nanorods are characterized by scanning electron microscopy (SEM) in which they are observed to have mean lengths and diameters of $l = 1.2$ μm and $d = 120$ nm, respectively [Fig. 1(a)].

B. Fresnel Lens Fiber Fabrication

A detailed description of the Fresnel lens fiber design and fabrication is given in Ref. [18]. The lenses are printed on standard, commercial single mode fibers (Nufern 780-HP) by femtosecond two photon lithography (Nanoscribe Photonic Professional GT) with commercial resist (Nanoscribe IP-Dip) [38]. The total writing time is 55 min for the lenses used in this work. To achieve a reasonable working distance at high NA, the optical fiber mode is expanded by propagation through a solid cylinder of 500 μm length [Fig. 1(b)]. The diffracting lens is modeled via a phase-function and geometrical ray-tracing based on the local grating approximation. The Fresnel lens fibers with NA = 0.5 produce a tightly focused Gaussian shaped spot with a waist of 0.8 μm at a focal distance of $f = 97.5$ μm in water.

C. Optical Trapping Setup

The schema of the optical fiber tweezers is displayed in Fig. 1(c). The 808 nm trapping laser (LU0808M250, Lumics) is separated into two equal arms using a polarizing beam splitter and a half-wave plate to control the relative light intensities in each arm. The light beam is coupled into the optical fibers using fiber launchers. The output power from each fiber is directly measured at its distal end in air, before and after each experiment. The power values given in this paper correspond to the emitted power of one fiber in air. The fibers are mounted on two sets of x, y, z piezoelectric translation stages for high precision position alignment (PI P-620 and SmarAct SLC-17 series). The trapping chamber consists of an O-ring placed in between two glass slides and cut in two parts to insert the fibers. All experiments are carried out at room temperature ($T = 290$ K).

A homemade microscope, consisting of a long working distance microscope objective (Mitutoyo G Plan Apo 50×, NA = 0.55) and a CMOS camera (Hamamatsu ORCA FLASH 4.0 LT), is used for trapping visualization. Typical trapping videos contain 3000 frames recorded at frame rates of 200 fps (frames per second). The Eu-doped nanorods are optically pumped using a 393.5 nm laser with a bandwidth below 1.5 nm (OxxiusLBX-395-120-CSB-PPA). The pump laser is injected directly through the microscope objective using a dichroic mirror. The pump laser polarization is not controlled, thus being oriented in an arbitrary direction inside the xy plane. The typical pump laser power is 25 mW at the output of the microscope objective.

The recorded trapping videos are analyzed using a custom-written particle tracking algorithm, developed in the Scilab environment. This algorithm is based on two-dimensional Gaussian fitting of the ellipsoidal trapped nanorod PL image. It takes into account the time dependent particle orientation in the observation plane. Two complementary methods are applied to deduce the trap stiffness κ from the particle position records, assuming a harmonic optical trapping potential

$U(x) = \frac{1}{2}\kappa x^2$ [6]. Both methods are used independently in the axial (x) and transverse (y) directions of the observation plane. In the Boltzmann statistics (BS) method, the probability P of finding the particle at position x can be described in the framework of the equipartition theorem by

$$P(x) = \frac{1}{Z} e^{-\frac{\kappa \cdot x^2}{2k_B T}}, \tag{1}$$

with Z the normalization factor and $2k_B T$ the thermal energy. In power spectrum analysis (PSA), the power spectrum of the recorded position is fitted to the Lorentzian function:

$$P(f) = \frac{2k_B T}{\gamma(f_c^2 + f^2)}, \tag{2}$$

with $f_c = \kappa/2\pi\gamma$ the corner frequency and γ the friction coefficient. To take into account the nonspherical shape of the trapped nanorods, the model developed by Tirado *et al.* is applied [39]. Two distinct friction coefficients, perpendicular and parallel to the nanorod long axis, are defined by

$$\gamma_\perp = \frac{4\pi \cdot l}{\ln p + \Gamma_\perp} \cdot \eta, \quad \gamma_{||} = \frac{2\pi \cdot l}{\ln p + \Gamma_{||}} \cdot \eta, \tag{3}$$

with $p = l/d$ the nanorod aspect ratio, η the dynamic viscosity [in water $\eta(300\,\mathrm{K}) = 8.65 \times 10^{-4}\,\mathrm{N \cdot s \cdot m^{-2}}$], and Γ a dimensionless correction coefficient depending on p. For the given aspect ratio ($p = 10$), these coefficients are $\Gamma_\perp = 0.86$ and $\Gamma_{||} = -0.11$, resulting in friction coefficients of $\gamma_\perp = 4.13 \times 10^{-9}\,\mathrm{N \cdot s \cdot m^{-1}}$ and $\gamma_{||} = 2.98 \times 10^{-9}\,\mathrm{N \cdot s \cdot m^{-1}}$, respectively.

For the spectroscopic measurements, the trapped nanorods' PL is collected through the microscope objective by introducing a mirror on a flip-mount. The emission is then directed onto either a spectrometer coupled to an EM-CCD camera (Princeton Instruments ProEM) or an avalanche photodiode (APD, Thorlabs APD440A) for lifetime measurements. A set of optical filters suppresses the trapping and pumping wavelengths. Moreover, a linear polarizer in front of the spectrometer allows us to record polarization-resolved emission spectra. The zero of the polarizer angle θ is experimentally calibrated to the direction parallel to the trapping fiber's axis. The emission spectra are recorded with a slit width of 0.88 mm and an integration time of 10 s. For lifetime measurements, the pump laser is directly modulated at 11 Hz with a rectangular waveform. The overall response time of the laser and the APD is ≈20 μs, well below the expected Eu^{3+} lifetime. The PL is acquired at the maximum APD gain of 2.65×10^9 V/W and without any spectral filtering. The lifetime τ of the $^5D_0$ level is obtained by fitting the normalized intensity to the single exponential function $I(t)/I_0 = \exp(-t/\tau)$, with I_0 the mean intensity at $t < 0$. To exclude any influence of the experimental setup, the numerical fits are limited to the time range from 500 μs to 10 ms.

3. RESULTS

A. Nanorod Trapping

$NaYF_4$:Eu nanorods are optically trapped in a counterpropagating geometry using two Fresnel lens fibers separated by 195 μm. Typical trapping powers are 11 mW to 32 mW. The PL image of the trapped nanorods shows elliptical bright spots with typical lengths and widths of 1.5 μm and 500–550 nm, respectively [Fig. 2(a)]. The spot width corresponds to the microscope resolution of ≈500 nm and does not indicate the actual nanorod width.

During trapping experiments, we concurrently observe untrapped nanorods that are attracted into the optical trap. When entering the trap, they form indistinguishable nanorod clusters with the rod(s) that is already trapped. In general, nanorods with high aspect ratios tend to form clusters of aligned nanorods that cannot be resolved by optical means. To get an estimation of the number of trapped particles, we measure the PL increase of the trapped cluster when a new nanorod joins [Fig. 2(a)]. The observed emission intensity steps are linearly increasing with the increasing number of nanorods in the clusters. It is thus possible to characterize the trapping properties as a function of the trapped cluster size.

Figure 2(b) shows the $x - y$ tracking record of clusters containing one, two, and three nanorods for a trapping laser power of 32.2 mW. As expected for counterpropagating two beam tweezers, the particles are more efficiently trapped in the direction transverse to the fibers, i.e., perpendicular to the laser beam axes. Moreover, the nanorods are mainly aligning parallel to the fiber axis. Finally, the trapping becomes more efficient with an increasing number of rods inside the cluster.

The position probability distribution in the transverse and axial directions depicts well the optical trap anisotropy [Fig. 2(c)]. The distributions fit well to Gaussian functions, thus allowing us to deduce the trap stiffness κ using BS (Fig. 4). The trap stiffness is linearly increasing with light power, as verified for trapping of one or three nanorods. The normalized trap stiffnesses, obtained by linear fitting through the origin, are given in Table 1. The trap stiffness is also obtained by applying PSA using two distinct Stokes' friction coefficients for the transverse and axial directions [Eq. (3)]. Good numerical fitting to the experimental results is found for nanorod diameters of 120 nm, 180 nm, and 240 nm for trapped clusters containing

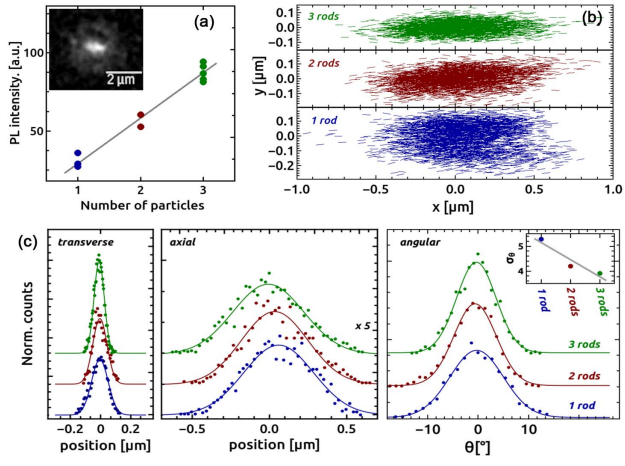

Fig. 2. Optical trapping results. (a) PL intensity as a function of the number of nanorods in the trapped cluster. Inset: microscope photoluminescence image of a trapped nanorod. (b) Particle tracking plot for one single nanorod and clusters of two or three rods ($P = 32.2$ mW). (c) Corresponding position (transverse and axial) and angular distributions. Inset: angular distribution width.

one, two, and three nanorods, respectively (Fig. 3). In the transverse direction, the actual fitting range of the power spectrum is limited from 2.5 Hz to 90 Hz. Experimental data presented in Fig. 4 and Table 1 are limited to videos with good agreement between experimental data and theory.

Depending on the number of nanorods in the trapped cluster, the trap stiffness is about 7 to 32 times higher in the transverse direction compared with the axial direction. This anisotropy increases significantly with the number of nanorods. In fact, the transverse trap stiffness for three rods is about 7.4 times higher than for a single rod, whereas the axial stiffness increase is limited to 1.6 times. Moreover, this dependency is quite different for the two directions (Fig. 4 insets). The increase is exponential in the transverse direction and exponentially converging towards a threshold in the axial direction.

The angular distribution width (σ_θ) is linearly decreasing with the number of particles [Fig. 2(c) and Table 1] and trapping power (not shown). The distribution width of 5.2° for one single rod at 32.2 mW trapping power is sufficiently low for the spectroscopic investigation of the anisotropic Eu^{3+} emission.

B. Photoluminescence of Optically Trapped Nanorods

The emission studies are performed on single nanorods and at a trapping power of 33.2 mW to ensure stable trapping with low angular dispersion. The emission spectrum exhibits three strong emission bands in the 570 nm to 710 nm spectral region [Fig. 5(a)]. One specific feature of the Eu^{3+} emission is the simultaneous presence of ED and MD transitions. Moreover,

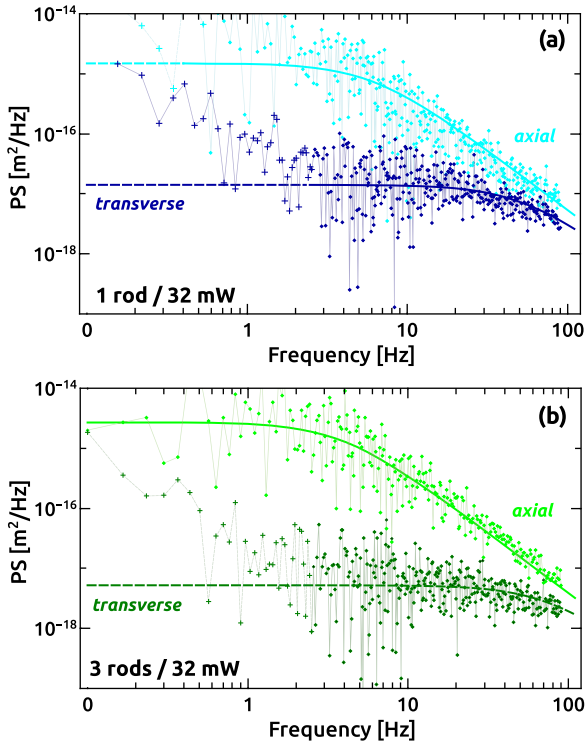

Fig. 3. Power spectrum analysis in axial and transverse directions for trapping of (a) one single rod and (b) a three-rod cluster. Lines are best fits to Eq. (2) (in the transverse direction, the fitting range is limited to frequencies $f > 2.5$ Hz).

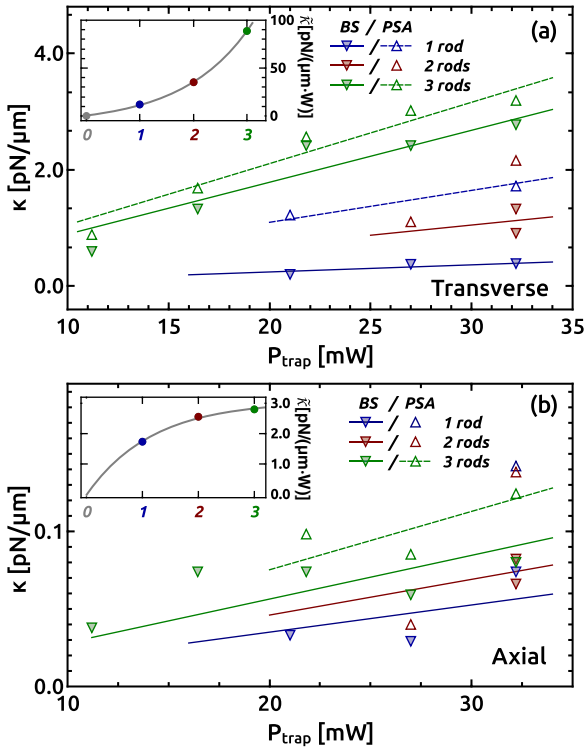

Fig. 4. Power dependent trap stiffness κ in the (a) transverse and (b) axial directions. The lines are linear fits through the origin to calculate the normalized trapping stiffness $\tilde{\kappa}$ shown in the insets as a function of number of nanorods in the trapped cluster (lines are guides to the eye; BS, Boltzmann statistics; PSA, power spectrum analysis).

Table 1. Transverse and Axial Normalized Trap Stiffness $\tilde{\kappa}$ Obtained by Boltzmann Statistics (BS) and Power Spectrum Analysis (PSA) and Angular Orientation Width σ_θ for One, Two, and Three Rods Trapped at $P = 32.2$ mW

	$\tilde{\kappa}$ [pN · μm^{-1} · W^{-1}]						
	BS			PSA			
	Trans.	Axial	Ratio	Trans.	Axial	Ratio	σ_θ
1 rod	12.2	1.74	7	48.3	–	–	5.2°
2 rods	35.0	2.55	13	–	–	–	4.2°
3 rods	89.3	2.81	32	106	3.76	28	3.9°

all main transitions start form the $^5D_0$ energy level: $^5D_0 \rightarrow {}^7F_1$ at 585–600 nm (MD_{590}), $^5D_0 \rightarrow {}^7F_2$ at 603–621 nm (ED_{615}), and $^5D_0 \rightarrow {}^7F_4$ at 683–705 nm (ED_{695}). The first transition is an MD transition, whereas the other two are ED transitions. The $^5D_0 \rightarrow {}^7F_3$ can be distinguished at about 650 nm. However, its low intensity makes its further characterization difficult. The further, relatively weak band at 582 nm corresponds to the $^5D_1 \rightarrow {}^7F_3$ transition, the only one starting from the higher $^5D_1$ level.

Each of the three main transition bands can be divided into three to four emission peaks with either π orientation ($\theta = 0°$, parallel to the fibers axis) or σ orientation ($\theta = 90°$, perpendicular to the fibers). As can be seen in Fig. 5, each transition band contains σ and π peaks. For example, the dominant

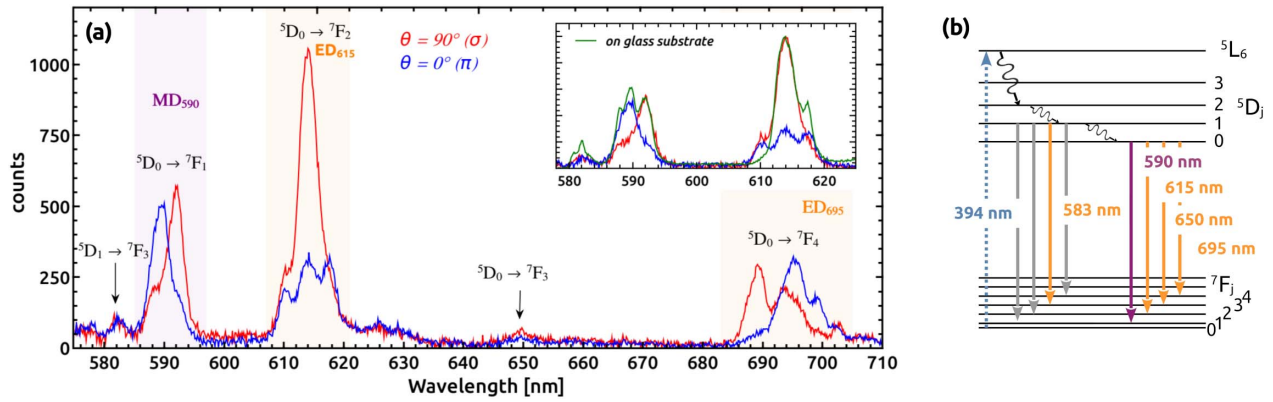

Fig. 5. (a) Emission spectra of optically trapped nanorods $NaYF_4:Eu^{3+}$ for σ and π orientations. Inset: comparison with the emission of nanorod clusters on a glass substrate. (b) Eu^{3+} energy level diagram.

contribution to the ED_{615} emission is of σ orientation with, however, a weak π oriented peak at 618 nm. In the case of the MD_{590} emission, two regions of similar intensity are distinguishable: π orientation below 590.5 nm and σ orientation for longer wavelengths. Finally, the ED_{695} band is of σ orientation at the low wavelength side and π orientation for longer wavelengths.

The emission spectra of trapped nanorods are compared to the emission of a single cluster of 15 to 20 nanorods on a glass substrate [Fig. 5(a) inset]. The linewidths of the emission peaks in the 575–630 nm range are identical for trapped and dispersed nanorods. The $^5D_1 \rightarrow {}^7F_3$ peak intensity is, however, more pronounced on the substrate. Moreover, the three MD_{590} peaks are better distinguishable, and the ED^1_{615} peak at 610 nm is missing in the cluster emission on the substrate.

For a more detailed study, emission spectra are recorded for polarizations from 0° to 180° in 15° steps. For each emission band, this set of 13 spectra is simultaneously fitted to three or four Gaussian curves [Figs. 6(a)–6(c)]. This method provides excellent agreement between the experimental and fitted data for all polarization angles. The respective peak positions and Gaussian width σ are listed in Table 2. Their emission orientation is revealed by means of polar plots of the Gaussian peak amplitudes [Figs. 6(d)–6(f)].

The experimental emission intensities are fitted to the orthogonal polar function:

$$I = A \cdot \sin^2(\theta - \varphi) + B \cdot \cos^2(\theta - \varphi), \tag{4}$$

with I the intensity, θ the polarizer angle with $\theta = 0°$ parallel to the trapping fibers' axes, and φ an angular shift that indicates the actual nanorod orientation with respect to the optical fiber axis (Table 2). For all clearly polarization dependent transitions, the deviation of the nanorod orientation from the

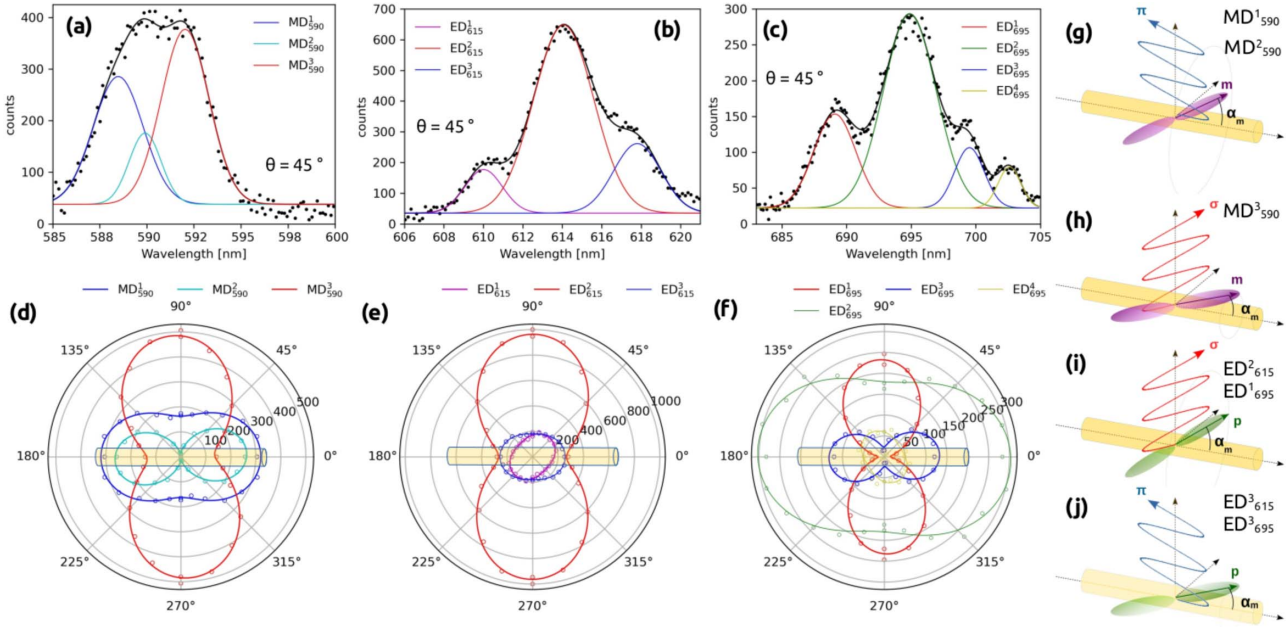

Fig. 6. Europium emission polarization properties. (a)–(c) Gaussian peak distribution applied for fitting the respective emission lines, (d)–(f) polar emission amplitude plots, and (g)–(j) schemes showing the respective electric and magnetic dipole orientations and main emission polarizations. The lines in the polar plots are best numerical fits to Eq. (4).

Table 2. Main Polar Fitting Parameters for Europium Emission Lines as Shown in Fig. 6[a]

Peak	Ori.	λ [nm]	σ [nm]	A	B	φ	α
MD^1_{590}	π	588.5	1.32	0.203	0.399	0.3°	63.2°
MD^2_{590}	π	589.9	0.85	0.027	0.486	3.2°	80.5°
MD^3_{590}	σ	592.0	1.27	0.642	0.179	3.7°	36.8°
ED^1_{615}	–	610.0	0.45	0.369	0.262	–43.7°	–
ED^2_{615}	σ	614.1	1.53	0.439	0.122	–0.3°	69.6°
ED^3_{615}	π	617.8	1.20	0.292	0.416	–0.2°	49.8°
ED^1_{695}	σ	689.1	1.62	0.485	0.302	2.7°	80.0°
ED^2_{695}	π	694.9	2.05	0.271	0.458	–3.3°	47.4°
ED^3_{695}	π	699.5	1.15	0.131	0.737	2.3°	30.8°
ED^4_{695}	–	702.6	0.88	0.375	0.249	32.6°	–

[a]A and B are normalized values.

trapping beam's axis is below 4°, in good agreement with the microscope observations.

ED and MD moments **p** and **m** are not perfectly parallel or perpendicular to the $NaYF_4$ c axis [34]. In the paraxial approximation, the angle α between the respective dipole moments and the c axis can be obtained from the fitting parameters A and B in Eq. (4) by using $A = \cos^2\alpha$ and $B = (1/2)\cdot\sin^2\alpha$ for an MD transition and $A = (1/2)\cdot\sin^2\alpha$ and $B = \cos^2\alpha$ for an ED transition [32]. In both cases, A and B have to be normalized using $\sin^2\alpha + \cos^2\alpha = 1$. Modeling the nanorod emission, one has to consider three orthogonal dipoles parallel to the rods' a, b, and c axes (parallel to the trap x, y, and z axes). As the emission is captured in the z direction only, half of the emission of the a and b dipoles is captured, leading to the factor 1/2 in front of A or B for ED and MD dipoles, respectively.

In the case of the MD transition, the two peaks MD^1_{590} and MD^2_{590} are of π orientation, whereas the MD^3_{590} peak is of σ orientation. The MD of the MD^2_{590} peak is orientated nearly parallel to the nanorod c axis ($\alpha = 80.5°$), resulting in a high B/A ratio and a narrow waist of its polar plot. On the other hand, the MD^1_{590} dipole orientation of 63.2° results in a more oval polar plot, which shows, however, still a clear π orientation. The dipole orientation of the MD^3_{590} peak ($\alpha = 36.8°$), well below 45°, reflects its σ orientation and results also in a clearly visible waist.

The ED_{615} emission band is dominated by the σ orientated peak ED^2_{615} with a dipole angle of $\alpha = 69.6°$. The dipole orientation of the longer wavelength peak ED^3_{615} of $\alpha = 49.8°$ is close to 45°, leading to a nearly oval polar plot. The short wavelength side peak ED^1_{695} does not show a clear orientation. Moreover, its fitted nanorod orientation angle of $\varphi = -43.7°$ prohibits the determination of the dipole orientation.

The ED_{695} emission band is the only one fitted to four Gaussian peaks. The long wavelength peak ED^4_{695} shows, however, no clear polarization behavior with $\varphi = 32.6°$. Moreover, the strongest peak (ED^2_{695}) shows less pronounced polarization dependence with a dipole orientation of $\alpha = 47.4°$. The two side peaks ED^1_{695} and ED^3_{695} show, however, strong σ and π orientation dependence with dipole angles of $\alpha = 80.0°$ and 30.8°, respectively.

The lifetime of the europium $^5D_0$ level is measured using a trapped nanorod cluster estimated to consist of two or three nanorods. The trapping conditions are equal to the ones for spectroscopic measurements. The PL decay is a single exponential with a lifetime of $\tau = 4.4$ ms (Fig. 7). No significant dependence on the pump power P_{pump} was observed in the 7–12 mW range. The PL emission power measured by the APD is linearly increasing with P_{pump}.

This PL decay of the trapped particles was compared to the already mentioned nanorod cluster on a glass slide. In this case, the decay is clearly a double exponential with short and long decay times of $\tau_1 = 1.3$ ms and $\tau_2 = 4.5$ ms, respectively. As for the trapped nanorods, no significant dependence is found between the pump power and the decay time, whereas the PL power increases linearly with P_{pump}.

4. DISCUSSION

Stable nanorod trapping is observed for fiber-to-fiber distances of about 200 μm and for light powers as low as 10 mW. As expected for dielectric nanorods, they align parallel to the beam/fiber axis, with a low angular distribution of $\sigma_\theta = 4°–5°$. The PSA suggests that the nanorod motion in the transverse and axial directions is not completely independent. In the transverse direction, the power spectra can be fitted to the Lorentzian function [Eq. (2)] only for frequencies above

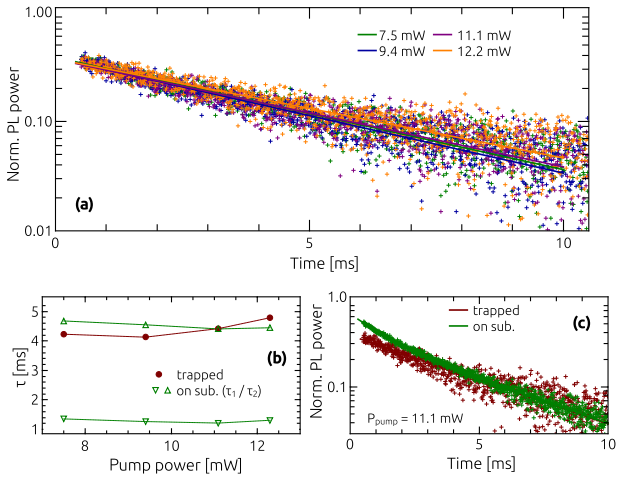

Fig. 7. (a) Photoluminescence (PL) decay for trapped nanorods at different pump powers. The lines are single exponential fits. (b) Pumper power dependent decay time. (c) PL decay for trapped nanorods and a nanorods cluster on a glass substrate.

2.5 Hz. At lower frequencies the power spectrum is not constant but approaches the value of the axial motion for frequencies of about 1 Hz. Taking into account the large aspect ratio of $p = 10$, the presence of weak rotational modes can provoke the coupling of the two linear translation modes at low frequencies.

In general, BS and PSA are complementary methods with each having its own advantages and drawbacks. BS does not require one to know the Stokes' friction coefficient. Slow mean trapping position shifts or two metastable trapping regions as observed for single rod trapping [Fig. 2(b)] result, however, in underestimated κ values. PSA allows one to neglect these drifts by fitting only to higher frequencies, but requires high frequency particle position recordings. In our case, the small nanorod PL signal limits video recordings to 200 fps. The linear slope of the PS above the corner frequency f_c can, thus, only be partially resolved (Fig. 3). As a consequence, the PSA was not possible for all trapping videos. Finally, the trap stiffness obtained by PSA is in general higher than the BS one. However, the trap efficiency and the angular distribution are largely sufficient for the study of the nanorod emission properties.

The observed polarization features of the Eu^{3+} emission are related to the intrinsic crystalline anisotropy and symmetry of lanthanide sites. The effect of birefringence on the polarized emission can be estimated to less than 1% for highly anisotropic crystals under the given experimental conditions. Chacon *et al.* studied the $NaYF_4$:Eu^{3+} emission by confocal microscopy on identical single nanorods, dispersed on a quartz substrate [32]. In accordance with our measurements on a glass substrate, they found a more intense $^5D_1 \rightarrow {}^7F_3$ transition peak at 583 nm and also three more pronounced peaks in the MD emission band. They determined the dipole orientations of the MD^{1-3}_{590} peaks to $\alpha = 65.7°$, 68.9°, and 37.8°, respectively. Compared to our present work, the MD of the MD^2_{590} peak was thus found to be about 10° smaller. The observed difference can be related to the influence of the quartz substrate on the Eu^{3+} emission properties.

In former work, we trapped $NaYF_4$:Eu^{3+} nanorods using optical fiber tips [37]. In this configuration, the nanorods were attracted to the fiber tips and trapping was realized with contact to one fiber tip. At that time, the spectroscopic study was limited to the MD_{590} and ED_{615} bands. The emission spectra are very similar in both cases. Using Fresnel lenses, the nanorods are, however, better aligned to the fiber axis. For a more detailed comparison, we have applied our advanced data analysis to the former results. Similar to the already mentioned nanorods on a quartz substrate, the MD orientation of the MD^2_{590} is found to be 5° smaller. Concerning the ED_{615} band, the polarization dependence of the short-wavelength side peak ED^1_{615} at 610 nm is less pronounced in the tip contact. The corresponding dipole angle of $\alpha = 51°$ is very close to 45°. As already mentioned, this peak is absent for nanorods dispersed on a substrate (Fig. 5 and Ref. [32]), suggesting that this feature is due to the contact with the optical fiber tip.

The PL decay of trapped nanorods is a single exponential with a decay time of 4.4 ms. For the particle cluster on the glass substrate, an additional, shorter decay with $\tau_1 = 1.3$ ms is observed. The appearance of this fast decay is not yet elucidated. It could be related to the stronger peak at 582 nm, which is the only observed emission line starting from the higher $^5D_1$ state. Nonradiative decay routes make the PL decay rate of this state considerably faster than that of the lowest excited state $^5D_0$ [27]. A further hypothesis could be dielectric influence of the substrate or even auto-fluorescence from the glass substrate.

5. CONCLUSION

Stable and reproducible trapping of europium-doped nanorods is studied in far-field, Fresnel lens dual fiber tweezers. High normalized trapping efficiencies $\tilde{\kappa}$ are observed for single nanorods or nanorod clusters containing two or three nanorods. PSA with distinct friction coefficients for the orthogonal directions parallel and perpendicular to the nanorod axis suggest slight coupling of the motion in these two directions.

Polarization-resolved spectroscopy allows us to specify the σ and π configurations of the ED and MD emission bands and to deduce the nanorod orientation. The Eu^{3+} emission decay time of 4–5 ms underlines the low phonon energy of the $NaYF_4$ host matrix.

The presented results highlight the outstanding performance of our Fresnel lens fiber optical tweezers, permitting stable trapping of nanoparticles at low light power and large particle to fiber distance. The optical study of free, purely optically trapped, single nanoparticles is significantly facilitated. Moreover, the possibility to determine the nanorod orientation by fast spectroscopic means is of paramount interest for microrheologic experiments with anisotropic particles.

Funding. Agence Nationale de la Recherche (ANR-16-CE24-0014-01); Okinawa Institute of Science and Technology Graduate University; Baden-Württemberg Stiftung (Operial); Bundesministerium für Bildung und Forschung (Printoptics); European Research Council (POC 3DPrintedOptics).

Acknowledgment. J.F acknowledges very fruitful discussions with G. Colas des Francs from ICB in Dijon, France. S. N.C. is grateful to Institut Néel for hosting her during the work. We thank also T. Pohl for his valuable help with graphics.

Disclosures. The authors declare no conflicts of interest.

Data Availability. Data underlying the results presented in this paper are not publicly available at this time but may be obtained from the authors upon reasonable request.

REFERENCES

1. A. Ashkin, J. M. Dziedzic, J. E. Bjorkholm, and S. Chu, "Observation of a single-beam gradient force optical trap for dielectric particles," Opt. Lett. **11**, 288–290 (1986).
2. A. Constable, J. Kim, J. Mervis, F. Zarinetchi, and M. Prentiss, "Demonstration of a fiber-optical light-force trap," Opt. Lett. **18**, 1867–1869 (1993).
3. J. S. Paiva, P. A. Jorge, C. C. Rosa, and J. P. Cunha, "Optical fiber tips for biological applications: from light confinement, biosensing to

bioparticles manipulation," Biochim. Biophys. Acta, Gen. Sub. **1862**, 1209–1246 (2018).
4. H. Lee, J. Park, and K. Oh, "Recent progress in all-fiber non-Gaussian optical beam shaping technologies," J. Lightwave Technol. **37**, 2590–2597 (2019).
5. X. Zhao, N. Zhao, Y. Shi, H. Xin, and B. Li, "Optical fiber tweezers: a versatile tool for optical trapping and manipulation," Micromachines **11**, 114 (2020).
6. J.-B. Decombe, S. Huant, and J. Fick, "Single and dual fiber nano-tip optical tweezers: trapping and analysis," Opt. Express **21**, 30521–30531 (2013).
7. A. Barucci, F. Cosi, A. Giannetti, S. Pelli, D. Griffini, M. Insinna, S. Salvadori, B. Tiribilli, and G. C. Righini, "Optical fibre nanotips fabricated by a dynamic chemical etching for sensing applications," J. Appl. Phys. **117**, 053104 (2015).
8. G. Leménager, K. Lahlil, T. Gacoin, G. Colas des Francs, and J. Fick, "Optical fiber tip tweezers, a complementary approach for nanoparticle trapping," J. Nanophoton. **13**, 012505 (2018).
9. Z. Liu, N. Zhang, Y. Tang, Y. Liu, and B. Zhang, "An optical fibre tip with double tapers etched by the interfacial layer," J. Mod. Opt. **66**, 168–175 (2019).
10. Y. X. Liu, B. Zhang, N. Zhang, and Z. L. Liu, "Fabricating fiber probes for optical tweezers by an improved tube etching method," Appl. Opt. **58**, 7950–7956 (2019).
11. Z. Xie, V. Armbruster, and T. Grosjean, "Axicon on a gradient index lens (AXIGRIN): integrated optical bench for Bessel beam generation from a point-like source," Appl. Opt. **53**, 6103–6107 (2014).
12. A. E. Eter, N. M. Hameed, F. I. Baida, R. Salut, C. Filiatre, D. Nedeljkovic, E. Atie, S. Bole, and T. Grosjean, "Fiber-integrated optical nano-tweezer based on a bowtie-aperture nano-antenna at the apex of a SNOM tip," Opt. Express **22**, 10072–10080 (2014).
13. R. S. Rodrigues Ribero, P. Dahal, A. Guerreiro, P. A. S. Jorge, and J. Viegas, "Fabrication of Fresnel plates on optical fibers by FIB milling for optical trapping; manipulation and detection of single cells," Sci. Rep. **7**, 4485 (2017).
14. J. M. Ehtaiba and R. Gordon, "Template-stripped nanoaperture tweezer integrated with optical fiber," Opt. Express **26**, 9607–9613 (2018).
15. R. S. Rodrigues Ribeiro, O. Soppera, A. G. Oliva, A. Guerreiro, and P. A. S. Jorge, "New trends on optical fiber tweezers," J. Lightwave Technol. **33**, 3394–3405 (2015).
16. K. Weber, F. Hütt, S. Thiele, T. Gissibl, A. Herkommer, and H. Giessen, "Single mode fiber based delivery of OAM light by 3D direct laser writing," Opt. Express **25**, 19672–19679 (2017).
17. M. Schmid, F. Sterl, S. Thiele, A. Herkommer, and H. Giessen, "3D printed hybrid refractive/diffractive achromat and apochromat for the visible wavelength range," Opt. Lett. **46**, 2485–2488 (2021).
18. A. Asadollahbaik, S. Thiele, K. Weber, A. Kumar, J. Drozella, F. Sterl, A. Herkommer, H. Giessen, and J. Fick, "Highly efficient dual-fibre optical trapping with 3D printed diffractive Fresnel lenses," ACS Photon. **7**, 88–97 (2020).
19. B. Agate, C. Brown, W. Sibbett, and K. Dholakia, "Femtosecond optical tweezers for *in-situ* control of two-photon fluorescence," Opt. Express **12**, 3011–3017 (2004).
20. C. Liberale, G. Cojoc, F. Bragheri, P. Minzioni, G. Perozziello, R. La Rocca, L. Ferrara, V. Rajamanickam, E. Di Fabrizio, and I. Cristiani, "Integrated microfluidic device for single-cell trapping and spectroscopy," Sci. Rep. **3**, 1258 (2013).
21. L. Anbharasi, E. Bhanu Rekha, V. Rahul, B. Roy, M. Gunaseelan, S. Yamini, V. N. Adusumalli, D. Sarkar, V. Mahalingam, and J. Senthilselvan, "Tunable emission and optical trapping of upconverting LiYF4:Yb, Er nanocrystal," Opt. Laser Technol. **126**, 106109 (2020).
22. S. Kumar, M. Gunaseelan, R. Vaippully, A. Banerjee, and B. Roy, "Breaking the diffraction limit in absorption spectroscopy using upconverting nanoparticles," Nanoscale **13**, 11856–11866 (2021).
23. R. Gillibert, G. Balakrishnan, Q. Deshoules, M. Tardivel, A. Magazzù, M. G. Donato, O. M. Maragò, M. Lamy de La Chapelle, F. Colas, F. Lagarde, and P. G. Gucciardi, "Raman tweezers for small microplastics and nanoplastics identification in seawater," Environ. Sci. Technol. **53**, 9003–9013 (2019).
24. C. Song, S. Zhang, Q. Zhou, H. Hai, D. Zhao, and Y. Hui, "Upconversion nanoparticles for bioimaging," Nanotechnol. Rev. **6**, 233–242 (2017).
25. A. Aebischer, M. Hostettler, J. Hauser, K. Krämer, T. Weber, H. U. Güdel, and H.-B. Bürgi, "Structural and spectroscopic characterization of active sites in a family of light-emitting sodium lanthanide tetrafluorides," Angew. Chem. Int. Ed. **45**, 2802–2806 (2006).
26. C. Liu, Y. Hou, and M. Gao, "Are rare-earth nanoparticles suitable for in vivo applications?" Adv. Mater. **26**, 6922–6932 (2014).
27. F. T. Rabouw, P. T. Prins, and D. J. Norris, "Europium-doped $NaYF_4$ nanocrystals as probes for the electric and magnetic local density of optical states throughout the visible spectral range," Nano Lett. **16**, 7254–7260 (2016).
28. D. Tu, Y. Liu, H. Zhu, R. Li, L. Liu, and X. Chen, "Breakdown of crystallographic site symmetry in lanthanide-doped $NaYF_4$ crystals," Angew. Chem. Int. Ed. **52**, 1128–1133 (2013).
29. R. Borja-Urby, L. Diaz-Torres, P. Salas, C. Angeles-Chavez, and O. Meza, "Strong broad green UV-excited photoluminescence in rare earth doped barium zirconate," Mater. Sci. Eng. B **176**, 1388–1392 (2011).
30. J. Kim, S. Michelin, M. Hilbers, L. Martinelli, E. Chaudan, G. Amselem, E. Fradet, J.-P. Boilot, A. M. Brouwer, C. N. Baroud, J. Peretti, and T. Gacoin, "Monitoring the orientation of rare-earth-doped nanorods for flow shear tomography," Nat. Nanotechnol. **12**, 914–919 (2017).
31. A. Parchur and R. Ningthoujam, "Behaviour of electric and magnetic dipole transitions of Eu^{3+}, $^5D_0 \rightarrow {}^7F_0$ and Eu-O charge transfer band in Li^+ co-doped YPO_4:Eu^{3+}," RSC Adv. **2**, 10859–10868 (2012).
32. R. Chacon, A. Leray, J. Kim, K. Lahlil, S. Mathew, A. Bouhelier, J.-W. Kim, T. Gacoin, and G. Colas des Francs, "Measuring the magnetic dipole transition of single nanorods by Fourier microscopy," Phys. Rev. Appl. **14**, 054010 (2020).
33. P. Rodríguez-Sevilla, L. Labrador-Páez, D. Wawrzyncyk, M. Nyk, M. Samoc, A. Kumar Kar, M. Mackenzie, L. Paterson, D. Jacque, and P. Haro-González, "Determining the 3D orientation of optically trapped upconverting nanorods by *in situ* single-particle polarized spectroscopy," Nanoscale **8**, 300–308 (2016).
34. J. Kim, R. Chacon, Z. Wang, E. Larquet, K. Lahlil, A. Leray, G. Colas des Francs, J. Kim, and T. Gacoin, "Measuring 3D orientation of nanocrystals via polarized luminescence of rare-earth dopants," Nat. Commun. **12**, 1943 (2021).
35. P. J. Reece, W. J. Toe, F. Wang, S. Paiman, Q. Gao, H. H. Tan, and C. Jagadish, "Characterization of semiconductor nanowires using optical tweezers," Nano Lett. **11**, 2375–2381 (2011).
36. G. Leménager, M. Thiriet, F. Pourcin, K. Lahlil, F. Valdivia-Valero, G. Colas des Francs, T. Gacoin, and J. Fick, "Size-dependent trapping behavior and optical emission study of $NaYF_4$ nanorods in optical fiber tip tweezers," Opt. Express **26**, 32156–32167 (2018).
37. A. Kumar, J. Kim, K. Lahlil, G. Julie, S. N. Chormaic, J. Kim, T. Gacoin, and J. Fick, "Optical trapping and orientation-resolved spectroscopy of europium-doped nanorods," J. Phys. Photon. **2**, 025007 (2020).
38. T. Gissibl, S. Wagner, J. Sykora, M. Schmid, and H. Giessen, "Refractive index measurements of photo-resists for three-dimensional direct laser writing," Opt. Mater. Express **7**, 2293–2298 (2017).
39. M. M. Tirado and J. Garcia de la Torre, "Translational friction coefficients of rigid, symmetric top macromolecules. Application to circular cylinders," J. Chem. Phys. **71**, 2581–2587 (1979).